

High Peak Power Tunable Visible Source at 550 nm from a Frequency Doubled Nanosecond Yb-doped Fiber MOPA

Jing He, Di Lin, Lin Xu, Martynas Beresna, Michalis N. Zervas, Shaif-ul Alam, and Gilberto Brambilla

Abstract— A high peak power tunable green source operating in the range of 544-552 nm is here demonstrated through frequency doubling a diode-seeded, nanosecond, polarization-maintaining, Yb-doped fiber master oscillator power amplifier system. Type-I second harmonic generation was implemented in a lithium triborate crystal via noncritical phase matching by temperature tuning. Narrow-bandwidth green light of average output power of up to 9 W, with a pulse duration of 1.8 ns and peak power of 25 kW, was obtained at a repetition rate of 200 kHz. The pump-to-green conversion efficiency reached 30%. This linearly polarized, narrow bandwidth, tunable source has great potential for applications such as material processing, sensing, and medical research.

Index Terms—Visible lasers, tunable lasers, optical fiber amplifiers, ytterbium, harmonic generation.

I. INTRODUCTION

HIGH power diffraction-limited visible sources with emission wavelengths of around 550 nm are in great demand for high-precision atomic and molecular research. This includes the absolute frequency measurement of molecular iodine at $\lambda \sim 548$ nm for lithium ion spectroscopy [1], laser cooled YbF molecules for measuring the electron electric dipole moment [2], and enhanced electron transfer for highly efficient hydrogen evolution [3]. In addition, sources operating in this spectral range also play important roles in molecular biology and medical diagnosis, as hemoglobin [4], red fluorescent protein DsRed [5], and several popular fluorescent dyes [6] have strong absorption in this range. Moreover, this wavelength range locates in the peak sensitivity of the human visual system [7] and is suitable for laser display and lighting. These sources can be realized using several approaches, such as sum-frequency mixing (SFM) of Nd:YAG and Nd:YVO₄ lasers [8], [9], Raman shifted pumped with a $\lambda \sim 532$ nm laser [10], and direct frequency doubling of lasers at 1.1 μm [11]. However, both the SFM process and Raman scattering processes require complicated optical setup,

which increase the complexity of the system, while frequency doubling generates only radiation at half the fundamental wavelength, which prevents its use in applications where the laser wavelength need to be specifically adjusted.

Rare-earth doped fiber lasers and amplifiers, in particular, Yb-doped fiber amplifiers (YDFAs) which exhibit a broad gain spectrum in the near-IR wavelength range around $\lambda \sim 1$ -1.15 μm [12], have proved to be ideal candidates to address these drawbacks. Compared with conventional solid-state lasers, fiber lasers usually provide better beam quality, improved compactness, and higher stability. Moreover, their exceptional efficiency and thermo-optical properties have allowed them to attain several kilowatts of output power [13]. Master oscillator power amplifier (MOPA) systems can thus take full advantage of both the diode laser seed, which provides flexible wavelength tuning and serves as a frequency selector, and the fiber amplifier, which allows for high brightness amplification over a wide range of wavelengths.

Additionally, by means of external cavity frequency conversion techniques, the spectral coverage of YDFAs can be extended to the visible range with similar advantages. A nonlinear crystal, such as lithium triborate (LBO) [14], β -Barium borate (BBO) [15] or a periodically poled nonlinear crystal [16], is normally employed in the single-pass configuration for second harmonic generation (SHG). However, frequency-doubled, high-power tunable pulsed green lasers operating around $\lambda \sim 550$ nm have rarely been reported to date. The difficulty originates in obtaining a powerful tunable source around of $\lambda \sim 1.1$ μm where emission is close to the edge of the ytterbium gain band. This necessitates a long active fiber to push the gain peak towards the longer wavelength edge and as such the maximum peak power extraction is primarily restricted by the nonlinear effects within the long device length.

Here we present a laser source tunable from $\lambda \sim 544$ -552 nm, by frequency doubling a fiberized, diode-seeded, polarization-maintaining (PM) YDFA MOPA system. High-peak-power pulse operation along with long-wavelength tunability were achieved by optimizing amplification stages to boost laser gain at $\lambda \sim 1.1$ μm whilst minimizing nonlinear effects. By using an LBO crystal featuring type-I noncritical phase matching (NCPM), SHG was achieved with an average output power up to 9 W. Short pulse with 1.8 ns duration and up to 25 kW peak power were obtained at a repetition rate of 200 kHz with a pump-to-green conversion efficiency as high as 30%.

Manuscript received ... This work was supported by the Engineering and Physical Sciences Research Council (EPSRC) (EP/L01243X/1 and EP/P027644/1), Royal Academy of Engineering Research Fellowship Scheme and Royal Academy of Engineering Research Chair Scheme.

All the authors are with Optoelectronics Research Centre, University of Southampton, Southampton, SO17 1BJ, U.K. (the corresponding author e-mail: J.He@soton.ac.uk).

The Data from this paper are accessible through the University of Southampton research depository <https://doi.org/10.5258/SOTON/D0818>.

II. EXPERIMENT SETUP

As depicted in Fig. 1, the system consists of a PM-fiber-pigtailed tunable seed, followed by a four-stage YDFA MOPA chain and a frequency doubling module.

The seed laser was based on a linearly polarized Fabry-Perot laser diode (Sacher Lasertechnik). The tunability of the seed signal was achieved by adjusting an internal diffraction grating with a linewidth of about 100 kHz, giving a working wavelength from 1088 nm to 1104 nm. The optical output of the seed laser was pre-shaped into Gaussian-like pulses using a high extinction ratio (>30 dB) electro-optic modulator (EOM) driven by an arbitrary waveform generator (AWG). The pulse width of the EOM output was set to 2 ns at a repetition rate of 5 MHz.

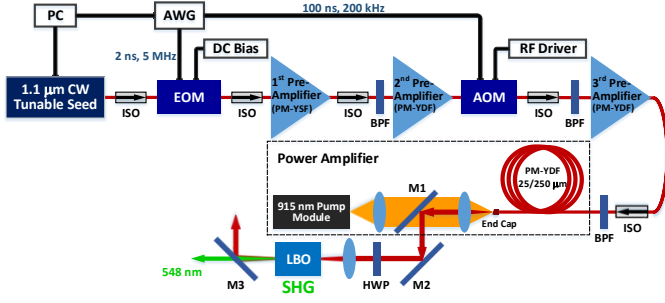


Fig. 1. Schematic diagram of the MOPA and the SHG system

Three preamplifiers were used to achieve sufficient signal power to seed the final-stage power amplifier. The first consisted of a 9 m long, core-pumped, PM Yb-doped fiber (YDF) with a core diameter of 5 μm and numerical aperture (NA) of 0.12. The type and length of the active fiber was chosen to provide maximum amplifier gain towards $\lambda \sim 1100$ nm. The amplifier was pumped in a co-propagating configuration by a 300 mW $\lambda \sim 976$ nm single-mode laser diode. A 0.3 mW seed signal from the EOM within the entire tuning wavelength range was amplified to an average output power of 10 mW with a gain of 15 dB. The output of the first stage amplifier was coupled into the second preamplifier stage via an in-line PM isolator (ISO) and a PM band-pass filter (BPF) with central wavelength of 1096 nm and a bandwidth of 16 nm (3 dB). Similar arrangements were adopted across the amplifier chain to prevent spurious lasing and to suppress the amplified spontaneous emission (ASE) at short wavelengths.

The second preamplifier comprised a 10m-long, double-clad PM YDF (PLMA-YDF-10/125-HI-8, Nufern), with a core/cladding diameter of 11.5/125 μm , and core/cladding NA of 0.08/0.46. This gain medium was pumped by a $\lambda \sim 915$ nm fiber-pigtailed broad-stripe diode laser through a fiberized pump combiner with maximum output power of 3 W. The output of this second-stage passed through a fiber-pigtailed acousto-optic modulator (AOM), which acts as an optical gate to remove excess ASE between the pulses and to reduce the repetition rate from 5 MHz to 200 kHz, in order to enable pulse energy scaling with moderate average output powers in the subsequent amplifiers. The third preamplifier, which used the same fiber parameters as the second, was thus seeded by a maximum average power of 10 mW due to the AOM insertion

loss and the pulse repetition frequency being reduced by a factor of 25. Its maximum average output power was 140 mW when the wavelength of the seed was set to 1088 nm.

The active fiber of the power amplifier stage was an 18 m long, cladding-pumped PM YDF (PLMA-YDF-25/250-VIII, Nufern) with a core/cladding diameter of 25/250 μm , and core/cladding NA of 0.06/0.46. Once again, the length of the active fiber in this stage was optimized by balancing the conflicting requirements of nonlinearity mitigation and short wavelength ASE suppression. Although the 25 μm core supports several transverse modes around $\lambda \sim 1 \mu\text{m}$, robust single mode operation was obtained by coiling the active fiber to a diameter of 75 mm to introduce additional bend-induced losses for the higher order modes. A 2 mm-long pure silica mode-expanding end-cap was spliced to the fiber output end and angle-polished to 8 degrees to avoid damage to the output facet and to prevent the backward-reflected power from coupling into the fiber core. An array of $\lambda \sim 915$ nm multi-mode laser diodes were then combined through a pump combiner to free-space end-pump the final amplifier.

The collimated MOPA output was frequency doubled by using an LBO crystal ($3 \times 3 \times 30$ mm³, $\theta = 90^\circ$, $\phi = 0^\circ$, EKSPA Optics) with Type I ($o_z^\omega + o_z^\omega \rightarrow e_{xy}^{2\omega}$) noncritical phase matching (NCPM). This crystal was chosen because of its excellent properties for SHG, which include high damage threshold, high nonlinear coefficient and broad transmission band. Furthermore, although NCPM of LBO varies with the fundamental wavelength, it can easily be addressed by temperature tuning. Finally, spatial walk-off does not occur in this setting, thus a diffraction-limited output beam could be generated. Prior to reaching the focusing lens, the orientation of the linearly polarized output of the YDF MOPA was rotated with the help of a half-wave plate (HWP) to adjust the polarization state in order to maximise conversion efficiency. Laser radiation was focused in the center of the crystal with a waist diameter of 90 μm corresponding to a Rayleigh range of 9 mm. The pump beam was intentionally focused smaller than the confocal parameter to improve the conversion efficiency [17]. The output from the LBO was passed through a dichroic mirror (DM) to filter out the unconverted fundamental pump radiation.

III. RESULT AND ANALYSIS

The length optimization of the gain fiber is critical for long wavelength operation. Different optimized lengths for different signal wavelengths have been reported using the same type of fiber, such as 0.85 m long fiber for $\lambda \sim 1034$ nm [18] and 3 m long fiber for $\lambda \sim 1060$ nm [14]. For the first preamplifier, we measured the forward ASE spectrum at different active fiber lengths but with the same pump power of 300 mW. The gain peak shifted to a longer wavelength (towards $\lambda \sim 1100$ nm) with increasing fiber length, changing from $\lambda \sim 1076$ nm to $\lambda \sim 1088$ nm when the fiber length increased from 10 m to 20 m, for example. The choice of ~ 10 m of gain fiber was a compromise between having sufficient gain at around $\lambda \sim 1100$ nm and minimizing nonlinear effects. Although the output of the first preamplifier was not located at

the maximum of the gain curve when seeded with a signal close to $\lambda \sim 1100$ nm (see Fig. 2), an effective amplification was achieved and an SNR of 35 dB was obtained, which is sufficient for seeding the following stages. Similar considerations were taken into account for the later stages, too.

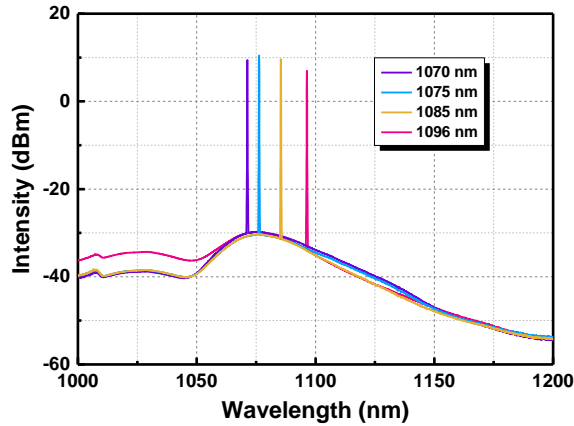


Fig. 2. Output Spectra of the first preamplifier with 300 mW, $\lambda \sim 976$ nm pumping, seeded at different signal wavelengths ($\lambda \sim 1070$, 1075, 1085 and 1096 nm)

The properties of the MOPA system are similar to those previously reported in [11]. To further investigate the features of SHG generated by the LBO crystal, the dependence of the SHG pulse energy (left-hand scale) and conversion efficiency (right-hand scale) on the input IR pulse energy were first investigated at a fixed wavelength of $\lambda \sim 1089$ nm (Fig. 3). The SHG pulse energy and conversion efficiency grow gradually with increasing input IR pulse energy. A maximum conversion efficiency of 64% and pulse energy of 45 μ J at $\lambda \sim 544.5$ nm were achieved at an IR pulse energy of 70 μ J. Observed saturation in conversion efficiency in the high IR energy region is attributed to thermal dephasing and frequency back-conversion. The pulses were slightly compressed to 1.8 ns after amplification and harmonic generation, giving a pulse peak power as high as 25 kW. During several hours of operation, no instabilities were observed in the green beam pattern from either optical damage or thermal lensing.

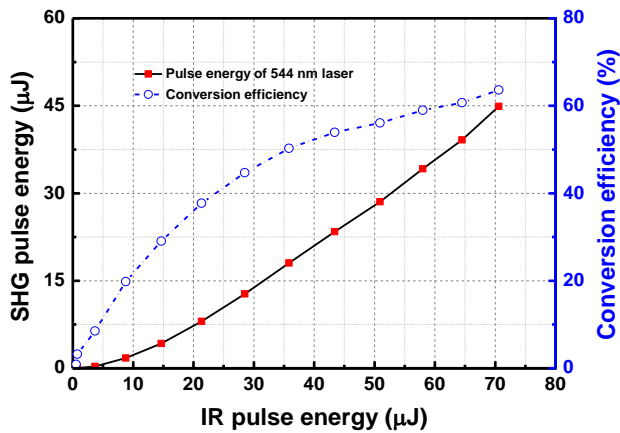


Fig. 3. Pulse energy and conversion efficiency of the SHG signal at $\lambda \sim 544.5$ nm as a function of the $\lambda \sim 1089$ nm fundamental power

To identify the NCPM temperature that maximizes the SHG output, temperature tuning curves were recorded at selected fundamental wavelength settings. The SHG output power was recorded whilst the temperature was changed and stabilized for a few minutes at a fixed incident IR power and wavelength. At the fundamental wavelength of 1089 nm, the NCPM temperature was found to be 123.35 ± 0.10 °C with a FWHM bandwidth of 1.30 °C. The measured data is well matched to the main peak of a $\text{sinc}^2(x)$ fit. NCPM temperatures were recorded at different wavelength settings to explore the relationship between the optimized NCPM temperature T and the fundamental wavelengths λ_{ω} . The results show that T decreases with increasing λ_{ω} . Apart from the quadratic fit, originating from the Sellmeier equations [19], a straight-line fit can be used to relate T to λ_{ω} : $T(\text{C}) = 1300.16673 - 1.08406 \times \lambda_{\omega}$, which gives a reasonable match with the data corresponding to the temperature tuning sensitivity of 1.08 °C/nm. The wavelength acceptance bandwidth was also measured by monitoring the SHG output as the fundamental wavelength was varied while maintaining the LBO crystal temperature at 123.35 ± 0.1 °C. The FWHM wavelength bandwidth was measured to be 1.2 nm in accordance with the calculated value.

The output spectra of the tunable green laser system are displayed in Fig. 4 (left-hand scale) for selected wavelengths. The laser output can be continuously tuned over a total bandwidth of 8 nm ranging from $\lambda \sim 544$ to 552 nm, corresponding to the 16 nm tuning range of the MOPA, which is limited by the bandwidth of the bandpass filter. The output spectra showed a bandwidth (measured at -20 dB level) of 0.15 nm and a signal-to-ASE ratio of more than 30 dB across the tuning range, measured with an optical spectrum analyzer (OSA, Yokogawa AQ6315A) with 0.05 nm resolution at different tuned wavelengths.

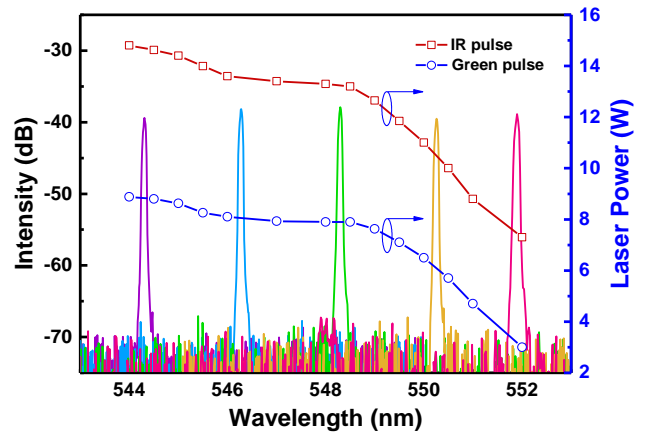


Fig. 4. Output spectra of the SHG and the corresponding average output power of IR and green pulsed laser within the tuning range

When the final power amplifier was pumped under the same conditions of 30 W launched power at $\lambda \sim 915$ nm, the obtained average output power of the fundamental light and SHG (Fig. 4, right-hand scale) was found to vary with tuning wavelength largely due to the variation in optical power of the fundamental signal. The maximum average output power of

SHG reached 9 W at $\lambda \sim 544$ nm, corresponding to a pump-to-green optical conversion efficiency of 30%. Further power scaling was primarily limited by self-phase modulation induced spectral broadening experienced by the amplified pulses as well as the transfer of energy to the SRS line. The decrease in observed SHG power at longer laser wavelengths can be explained by taking into account the ytterbium-doped silica fiber quantum defect and emission cross section. Steep drop of the SHG power at wavelengths longer than $\lambda \sim 549$ nm was attributed to the fast build-up of ASE in the MOPA chain. In fact, ASE grows much more rapidly at the longer wavelength side of the emission spectrum of the ytterbium in comparison to the weaker gain band of the amplified signal. Thus it consumes much of the pump energy, leading to a significantly degraded signal-to-ASE ratio. For example, the power of the amplified fundamental signal varied from 14.1 W at $\lambda \sim 1088$ nm to 7.3 W at $\lambda \sim 1104$ nm. The incorporation of a tunable filter with/without adjustable spectral width around $\lambda \sim 1100$ nm range offers a potential solution to this problem, as it will limit the band of ASE seeded to the following stage and allows the further extension of the tuning range.

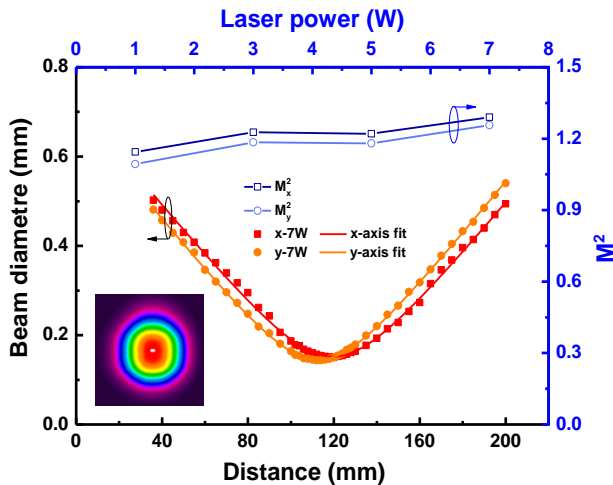


Fig. 5. Measured beam quality (M^2) at 7 W of SHG power (inset: Near-field beam profile), and dependence of the M^2 on SHG power at 545 nm

A scanning slit profiler (NS2s-Pyro/9/5, Ophir) was used to measure the beam quality of the SHG signal which was based on $D4\sigma$ method. The M^2 factor of the frequency doubled green signal at $\lambda \sim 545$ nm (left-hand scale of Fig. 5) was measured to be 1.29 (x-axis) and 1.26 (y-axis) with a Gaussian-distribution far-field beam profile (inset in Fig. 5) at 7 W output power. The variation in M^2 parameter with average output power of the $\lambda \sim 545$ nm signal is also plotted in Fig. 5 (right-hand scale), indicating a small degradation in beam quality from 1.14 to 1.29 (x-axis) and 1.09 to 1.26 (y-axis) when the power increased from 1 W to 7 W.

IV. CONCLUSION

In summary, we have demonstrated a linearly polarized, narrow-bandwidth, green laser tunable from $\lambda \sim 544$ to 552 nm with a 1.8 ns pulse duration and up to 25 kW pulse peak power, by frequency doubling a fiberized, diode-seeded, PM YDFA MOPA system. The SHG was achieved by temperature

tuning an LBO crystal featuring type-I noncritical phase matching, providing an average output power of up to 9 W with an IR-to-green conversion efficiency as high as 64% and a pump-to-green conversion efficiency of up to 30%. This linearly polarized, narrow bandwidth, tunable source can offer potential solutions for many applications, such as material processing, optical communications, and spectroscopy.

REFERENCES

- [1] Y. Hsiao, C. Kao, H. Chen et al., "Absolute frequency measurement of the molecular iodine hyperfine transitions at 548 nm," *J. Opt. Soc. Am. B: Opt. Phys.*, vol. 30, no. 2, pp. 328-332, Feb. 2013.
- [2] J. Lim, J. Almond, M. Trigatzis et al., "Laser Cooled YbF Molecules for Measuring the Electron's Electric Dipole Moment," *Phys. Rev. Lett.*, vol. 120, no. 12, Mar. 2018.
- [3] S. Min, and G. Lu, "Enhanced Electron Transfer from the Excited Eosin Y to mpg-C₃N₄ for Highly Efficient Hydrogen Evolution under 550 nm Irradiation," *J. Phys. Chem. C*, vol. 116, no. 37, pp. 19644-19652, Sep. 2012.
- [4] Y. Seto, M. Kataoka, and K. Tsuge, "Stability of blood carbon monoxide and hemoglobins during heating," *Forensic Sci. Int.*, vol. 121, no. 1-2, pp. 144-150, Sep. 2001.
- [5] T. Hawley, W. Telford, A. Ramezani et al., "Four-color flow cytometric detection of retrovirally expressed red, yellow, green, and cyan fluorescent proteins," *BioTechniques*, vol. 30, no. 5, pp. 1028+, May 2001.
- [6] M. Taniguchi, and J. Lindsey, "Database of Absorption and Fluorescence Spectra of > 300 Common Compounds for use in PhotochemCAD," *Photochem. Photobiol.*, vol. 94, no. 2, pp. 290-327, Mar. 2018.
- [7] F. Zaidi, J. Hull, S. Peirson et al., "Short-wavelength light sensitivity of circadian, pupillary, and visual awareness in humans lacking an outer retina," *Curr. Biol.*, vol. 17, no. 24, pp. 2122-2128, Dec. 2007.
- [8] Y. Wu, X. Zhang, and G. Sun, "All-solid-state doubly resonant sum-frequency mixing laser at 555 nm," *Laser Phys.*, vol. 21, no. 6, pp. 1074-1077, Jun. 2011.
- [9] J. Guo, H. Zhu, S. Chen et al., "Yellow, lime and green emission selectable by BBO angle tuning in Q-switched Nd:YVO₄ self-Raman laser," *Laser Phys. Lett.*, vol. 15, no. 7, Jul. 2018.
- [10] R. Mildren, M. Convery, H. Pask et al., "Efficient, all-solid-state, Raman laser in the yellow, orange and red," *Opt. Express*, vol. 12, no. 5, pp. 785-790, Mar. 2004.
- [11] J. He, D. Lin, L. Xu et al., "5.6 kW peak power, nanosecond pulses at 274 nm from a frequency quadrupled Yb-doped fiber MOPA," *Opt. Express*, vol. 26, no. 6, pp. 6554-6559, Mar. 2018.
- [12] R. Paschotta, J. Nilsson, A. Tropper et al., "Ytterbium-doped fiber amplifiers," *IEEE J. Quantum Electron.*, vol. 33, no. 7, pp. 1049-1056, Jul. 1997.
- [13] M. Zervas, and C. Codemard, "High Power Fiber Lasers: A Review," *IEEE J. Sel. Top. Quantum Electron.*, vol. 20, no. 5, Sep. 2014.
- [14] K. Chen, S. Alam, J. Hayes et al., "56-W Frequency-Doubled Source at 530 nm Pumped by a Single-Mode, Single-Polarization, Picosecond, Yb³⁺-Doped Fiber MOPA," *IEEE Photon. Technol. Lett.*, vol. 22, no. 12, pp. 893-895, Jun. 2010.
- [15] C. Rothhardt, J. Rothhardt, A. Klenke et al., "BBO-sapphire sandwich structure for frequency conversion of high power lasers," *Opt. Express Materials*, vol. 4, no. 5, pp. 1092-1103, May 2014.
- [16] F. Kontur, I. Dajani, Y. Lu et al., "Frequency-doubling of a CW fiber laser using PPKTP, PPMgSLT, and PPMgLN," *Opt. Express*, vol. 15, no. 20, pp. 12882-12889, Oct. 2007.
- [17] G. Boyd, and D. Kleinman, "Parametric Interaction of Focused Gaussian Light Beams," *J. Appl. Phys.*, vol. 39, no. 8, pp. 3597-3639, 1968.
- [18] H. Chan, S.-u. Alam, L. Xu et al., "Compact, high-pulse-energy, high-power, picosecond master oscillator power amplifier," *Opt. Express*, vol. 22, no. 18, pp. 21938-21943, Sep. 2014.
- [19] T. Ukachi, R. J. Lane, W. R. Bosenberg et al., "Phase-matched second-harmonic generation and growth of a LiB₃O₅ crystal," *J. Opt. Soc. Am. B: Opt. Phys.*, vol. 9, no. 7, pp. 1128-1133, Jul. 1992.